Desalination and Water Treatment
www.deswater.com

doi: 10.5004/dwt.2021.27109

222 (2021) 92–102
May

Design optimization and sensitivity analysis of a hybrid renewable power generation system coupled with a reverse osmosis desalination unit

Habib Cherif[a,b,*], Jamel Belhadj[a,b]

[a]*Université de Tunis, ENSIT, B.P. 56 Montfleury, 1008, Tunis, Tunisia, Tel. +216-97-409-503; Fax: +216-71-872-729; emails: habib.echrif@fsgf.u-gafsa.tn (H. Cherif), jamel.belhadj@ensit.rnu.tn (J. Belhadj)*
[b]*Université de Tunis El Manar, LSE/ENIT, B.P. 37 le Belvédère 1002, Tunis, Tunisia*

Received 10 August 2020; Accepted 2 February 2021

ABSTRACT

This paper presents a multi-criteria optimization based on parametric sensitivity analysis for the sizing of a hybrid renewable production system (photovoltaic-wind) coupled to a water pumping and reverse osmosis water desalination unit. A dynamic simulator of the proposed system which includes photovoltaic-wind (PV/wind) renewable generators, three motor-pumps (well pumping, water storage and desalination), reverse osmosis desalination unit, three water tanks, annual consumption data of freshwater with a sampling step of 10 min, annual data of weather conditions (Southern Tunisia), energy management and life cycle analysis indicators is developed. An energy management strategy is integrated into a dynamic simulator in order to share the power flow during the system operation. A parametric sensitivities-optimization method based on a genetic algorithm allows us to find the best configuration between the PV array areas, the wind turbine swept area and the capacity of the storage tanks with a reduced process time. The best configuration is predicted on the basis of the minimum primary energy requirement (environmental indicator) with an Loss of Power Supply Probability equal to 0% (reliability indicator). As a result, optimization based on sensitivity analysis is a good way to make the system more effective and run more smoothly.

Keywords: Renewable energy; Hybrid PV/wind system; Energy management; Optimization; Parametric sensitivity; Desalination

1. Introduction

With climate change and the growth of the world population, the need for electricity and freshwater has steadily increased and research into non-polluting energy sources has become nowadays more and more urgent. In fact, it is necessary to use renewable/green energies in global electricity generation, which constitute a viable alternative to fossil fuels especially in dry regions and isolated areas of the world [1–4]. Increasing the share of renewable resources for electricity generation can reduce the environmental impacts in terms of embodied energy and total greenhouse gas emissions and reduce the dependency on fossil fuels. The environmental impacts are assessed via the life cycle analysis (LCA) method [5]. To meet these challenges, environmental considerations must be integrated into systems design and the use of hybrid systems based on renewable energy sources such as wind and solar can play an important role in providing electricity and/or matter (water, hydrogen) to the billions of people who depend on traditional sources of energy [6–10]. Hence, it is more reliable and efficient to install a hybrid photovoltaic-wind system in which the complementary characteristics of solar and wind energies are combined. Also, for sustainable development, renewable energy sources are the solution to supply such water treatment process especially in remote rural areas with low infrastructure and no grid connection as certain coastal areas, islands or isolated areas in large deserts. It is then essential to focus on solar and wind energies coupled to desalination

* Corresponding author.

(renewable energy-desalination nexus) with the objective to reduce environmental impacts.

The sizing of renewable hybrid systems is a complex issue, especially coupled with several water pumping and desalination processes (hydraulic load), which depend on the weather conditions (intermittent renewable energy sources). In this regard, Zhou et al. [11] studied the optimal operation approach using a multi-objective hydroelectric power system equipped with a seawater reverse osmosis desalination station. The genetic algorithm is used to effectively reduce the costs of desalinated water. Mehrjerdi [12] studied the optimization of a water-energy system powered by a hybrid renewable source. The permeate water is produced by the desalination units. The author discussed the optimization problem which is based on homer software in order to find minimum costs of the system while guarantees a predefined level of supply reliability. Maleki et al. [13] proposed the weather forecasting for optimization of a hybrid solar/wind system coupled to a reverse osmosis desalination unit with battery storage. The optimal capacities for the discussed system are investigated in terms of life cycle cost and loss of power supply probability via a harmony search-based chaotic search algorithm. Zhang et al. [14] studied the design optimization method of small reverse osmosis (RO) desalination systems powered by wind and solar energies. Three configurations are introduced: solar-wind-RO desalination with battery storage, wind-RO desalination with battery storage and solar-RO desalination with battery storage. The optimization process aims to minimize the life cycle cost and reliability. For this aim, the simulated annealing-chaotic search algorithm is used.

In the mentioned literature, sizing optimization is always done using optimization algorithms that require a high CPU time: some authors use a simulation including the physical equations of each element which is done with a computing step of several hours or days especially with large time scale systems.

Inspired by the aforementioned published work, the main contributions of this paper are: (1) a configuration of hybrid photovoltaic-wind system coupled to a water pumping and brackish water desalination unit with hydraulic storage is introduced, and a dynamic simulator of the proposed system coupled with an energy management loop and its environment (solar irradiation, wind speed, consumption profiles, water flow in storage) is developed under MATLAB/SIMULINK and exploited; (2) a parametric sensitivity study is developed to handle the hybrid system design with water desalination in order to set the range of optimization parameters and consequently reduce the CPU time; (3) based on the parametric sensitivity, the optimum sizing of the hybrid energy system with desalination is developed using multi-objective optimization (embodied energy for environmental evaluation and loss of power supply probability for the reliability) and solved by both the genetic algorithm (GA) and Pareto dominance schemes, namely, NSGA-II Algorithm.

The remainder of the paper is organized as follows: Section 2, modeling of hydraulic process powered by the hybrid renewable system is presented. Section 3 describes the energy management strategy. Next, respectively in Sections 4 and 5, the parametric sensitivity method and a multi-criteria optimization for the sizing of hybrid renewable production systems are presented and explained. Section 6 presents the analysis of the results. Finally, conclusions are presented in Section 7.

2. Modeling of hydraulic process powered by hybrid PV/wind source

The considered system is a hybrid photovoltaic-wind system coupled to, via a DC bus link, a water pumping and desalination unit without battery storage (Fig. 1). The absence of electrochemical storage is the particularity of this system; only hydraulic storage is used to distribute freshwater to consumers [15]. The hybrid system is coupled to a DC bus through power converters. The hydraulic process is based on pumping brackish water from a well by an immersed motor-pump P1, high-pressure desalination motor-pump P2 in order to supply reverse osmosis (desalination unit) and pumping freshwater to a higher position (water tower) by a motor-pump P3. So, the hydraulic process is composed of three motor-pumps, a desalination unit with stages of pressure vessels (FilmTec membrane elements) and three water tanks. Infact, FilmTec Corp, a subsidiary of US-based Dow Chemical Co, has released version 6.0 of its Reverse Osmosis System Analysis (ROSA) design software. The Location for this company is: Dow Corporate Headquarters 2211 H.H. Dow Way Midland, MI 48674. The applied desalination technology of the proposed system is a reverse osmosis (RO) process [16,17]. RO technique is characterized by lower energy demand, lower cost and improved membrane durability compared to other desalination technologies as multi-effect distillation and multi-stage flash [18].

2.1. Components of the hybrid power source

2.1.1. Solar module

Output electric power from the photovoltaic generator depends on the incident radiation and the cell temperature [19,20]. Output electric power is given by:

$$P_{\mathrm{PV}} = \eta_{\mathrm{PV}} \times A_{\mathrm{PV}} \times G_T. \tag{1}$$

where η_{PV} is the power conversion efficiency of the PV panel, A_{PV} is the surface area of the PV panels, G_T is the solar radiation on tilted surface. The power conversion efficiency is given by the study of Hysa [21].

$$\eta_{\mathrm{PV}} = \eta_{\mathrm{mp,STC}}\left(1 + \alpha_p\left(T_c - T_{c,\mathrm{STC}}\right)\right). \tag{2}$$

where α_p is the temperature coefficient of the power, $T_{c,\mathrm{STC}}$ is the PV cell temperature under standard test conditions, $\eta_{\mathrm{mp,STC}}$ is the maximum power point efficiency of the PV module under standard test conditions, T_c is the PV cell temperature.

According to the solar radiation G_T and the ambient temperature T_a (°C), the PV cell temperature can be computed by the following empirical expression [20].

$$T_c = 30 + 0.0175 \times \left(G_T - 300\right) + 1.14 \times \left(T_a - 25\right) \tag{3}$$

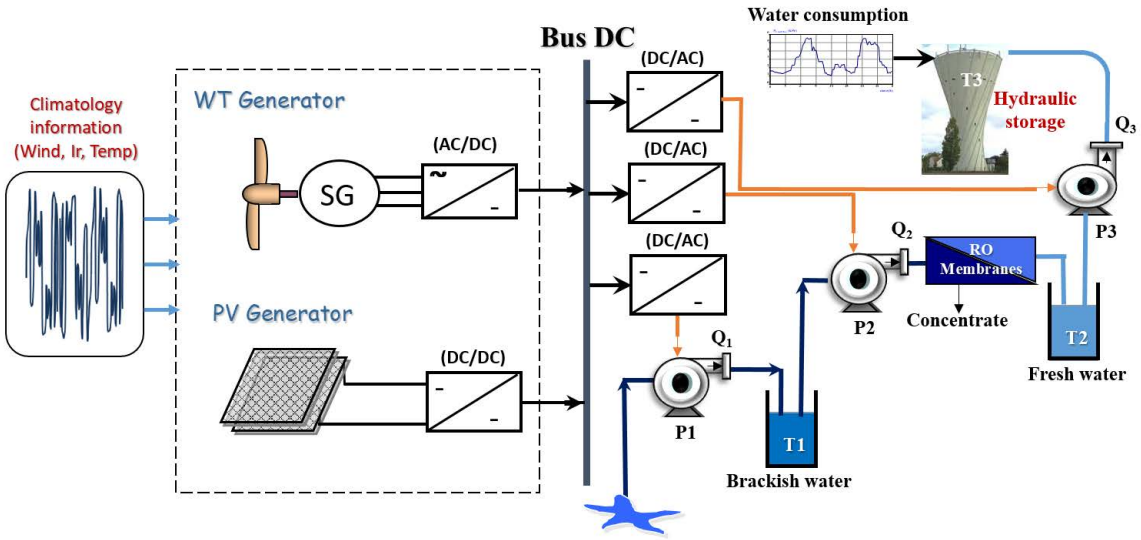

Fig. 1. Hybrid renewable production system coupled to a reverse osmosis desalination unit.

2.1.2. Wind turbine

The electrical power output of a wind generator is expressed by Layadi et al. [22].

$$P_{WT} = 0.5 \times \rho \times A_{WT} \times C_p \times \eta_g \times V^3 \quad (4)$$

where V is the wind speed (m/s), C_p is the optimal wind turbine power coefficient, A_{WT} is the turbine surface area (m²) and ρ is air density (kg/m³).

2.2. Components of the hydraulic process

The hydraulic process includes three combinations of motor-pumps with different functions: pumping brackish well water, desalination and pumping freshwater to the water tower. The motor pumps will be operated within a certain range of their input power with high efficiencies (variable frequency). In particular, it is important to respect pumping power limits to prevent problematic operations which degrade efficiency and which also reduce the lifetime of pumps.

2.2.1. Desalination pump

The pump P2 (vertical multi-stage centrifugal pump for RO) is rated at 7.5 kW (Grundfos type CRN 10–21 SF, Grundfos Holding A/S Poul Due Jensens vej 7 8850 Bjerringbro, Denmark) to increase pressure and deliver freshwater from T1 to T2 through the RO module. The operation point is the intersection point between the pump characteristic with the load characteristic. With the help of WinCAPS software for pumps [23], Fig. 2 describes the static head vs. output flow for different frequencies of pump P2 with the hydraulic load. With the "curve fitting tool" of MATLAB, the hydraulic load characteristic can be approximated by:

$$H_2 = 50 + 1.05 \times Q_2^2. \quad (5)$$

where H_2 is the static head (m) (total height) and Q_2 is the output flow (m³/h) of the pump P2.

According to Grundfos manufacturer data (Grundfos Holding A/S Poul Due Jensens vej 7 8850 Bjerringbro, Denmark) [23], the output flow characteristic vs. mechanical power of the pump P2 for different frequencies (different values of rotor speed) is presented in Fig. 3. Note that the frequency varies between 50 Hz (16.3 × 10⁵ Pa) and 32.6 Hz (8 × 10⁵ Pa). The range of frequency variation is limited by the osmotic pressure of the desalination unit and by the fouling factor of the RO FilmTec membrane elements. The output flow – mechanical power relation is expressed by:

$$Q_2 = 4.08 \times P_{m2}^{0.49}. \quad (6)$$

where P_{m2} is the mechanical power of the pump P2.

In fact, the shared power assigned to P2 has to be bounded (maximum input power and minimum input power) by:

$$\begin{cases} P_{m2\max} = 6.9 \text{ kW} \\ P_{m2\min} = 1.9 \text{ kW} \end{cases} \quad (7)$$

2.2.2. Well pump

Submerged pump P1 is valued at 3.5 kW to supply brackish water to tank T1 from the well with a static height of 16.5 m (Grundfos SP 14A-10, Grundfos Holding A/S Poul Due Jensens vej 7 8850 Bjerringbro, Denmark). With the help of WinCAPS software for pumps [23], Fig. 4 presents the static head vs. output flow for different frequencies of pump P1 with the load characteristic. The hydraulic load characteristic is approximated by:

$$H_1 = 16.5 + 0.15 \times Q_1^2. \quad (8)$$

where H_1 is the static head (m) (total height) and Q_1 is the output flow (m³/h) of the pump P1.

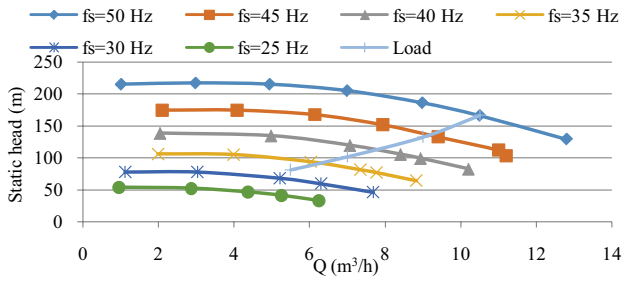

Fig. 2. Characteristic of pump P2 CRN 10-21 SF (Grundfos, Grundfos Holding A/S Poul Due Jensens vej 7 8850 Bjerringbro, Denmark) with load characteristic.

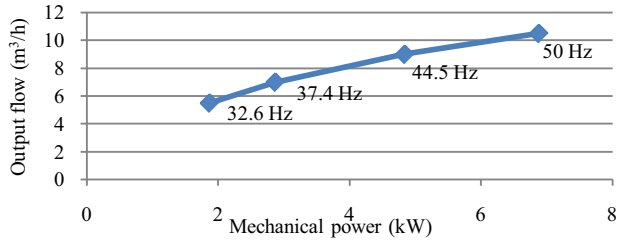

Fig. 3. The output flow of the pump P2 vs. mechanical power with variable speeds.

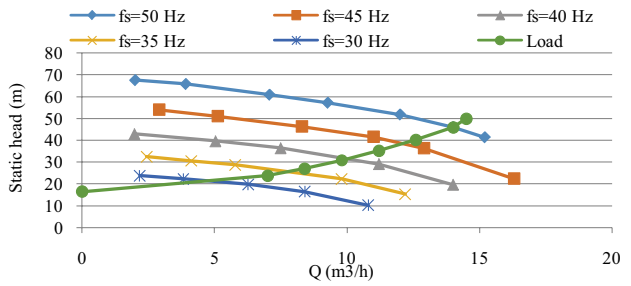

Fig. 4. Characteristic of pump P1 SP 14A-10 (Grundfos, Grundfos Holding A/S Poul Due Jensens vej 7 8850 Bjerringbro, Denmark) with load characteristic.

The intersection of the static head (for different frequencies) with the load curve gives the operating points. Accordingly, the output flow characteristic vs. mechanical power of the pump P1 for different frequencies is presented in Fig. 5. The frequency varies between 50 Hz (4.6×10^5 Pa) and 39.6 Hz (3×10^5 Pa). With the "curve fitting tool" of MATLAB, a custom flow–mechanical power model can depict these combinations by:

$$Q_1 = 8.35 \times P_{m1}^{0.47}. \quad (9)$$

where P_{m1} is the mechanical power of the pump P1.

In fact, the boundaries of mechanical power variation are given by:

$$\begin{cases} P_{m1\max} = 3 \text{ kW} \\ P_{m1\min} = 1.5 \text{ kW} \end{cases} \quad (10)$$

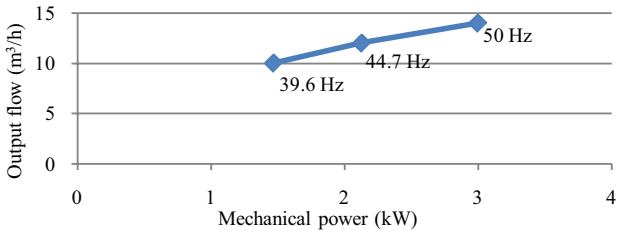

Fig. 5. The output flow of the pump P1 vs. mechanical power with variable speeds.

Taking into account the power management between the three pumps and to avoid overlap between the pumps P1 and P3, the power of the pump P1 was limited between 3 kW (50 Hz) and 1.5 kW (39.6 Hz). In addition, the minimum frequency is limited by the hydraulic pump efficiency.

2.2.3. Storage pump

Pump P3 is rated at 2 kW (Grundfos type CRTE-4-8, Grundfos Holding A/S Poul Due Jensens vej 7 8850 Bjerringbro, Denmark) to store freshwater in tank T3 (Water Tower) from tank T2 with a static height of 20 m. With the help of WinCAPS software for pumps [23], Fig. 6 presents the static head vs. output flow for different frequencies of pump P3 with the load characteristic. From Fig. 6 and with the help of the "curve fitting tool" of MATLAB, the hydraulic load characteristic can be approximated by:

$$H_3 = 20 + 0.83 \times Q_3^2. \quad (11)$$

where H_3 is the static head (total height of the pump P3) and Q_3 is the output flow of the pump P3.

According to Grundfos manufacturer data (Grundfos Holding A/S Poul Due Jensens vej 7 8850 Bjerringbro, Denmark) [23], the intersection of the static head with the load curve gives the mechanical power at different frequencies. The output flow characteristic vs. mechanical power of the pump P3 for different frequencies is presented in Fig. 7. The frequency varies between 50 Hz (5×10^5 Pa) and 33.2 Hz (2.7×10^5 Pa). Using the "curve fitting tool" of MATLAB, the flow–mechanical power relation is expressed by:

$$Q_3 = 4.80 \times P_{m3}^{0.59}. \quad (12)$$

where P_{m3} is the mechanical power of the pump P3.

In fact, the boundaries of mechanical power variation are given by:

$$\begin{cases} P_{m3\max} = 1.5 \text{ kW} \\ P_{m3\min} = 0.4 \text{ kW} \end{cases} \quad (13)$$

It is important to note that the minimum frequency is limited by the hydraulic pump efficiency.

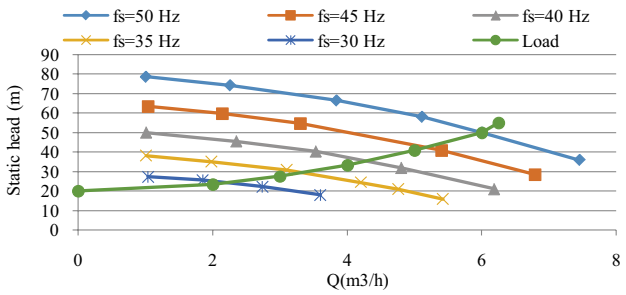

Fig. 6. Characteristic of pump P3 CRTE-4-8 (Grundfos, Grundfos Holding A/S Poul Due Jensens vej 7 8850 Bjerringbro, Denmark) with load characteristic.

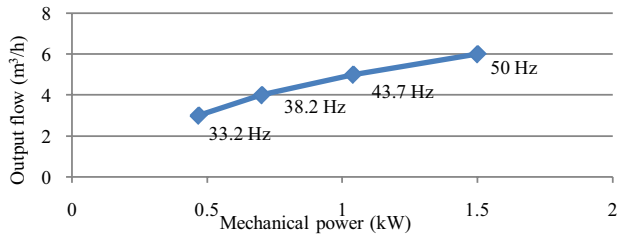

Fig. 7. The output flow of the pump P3 vs. mechanical power with variable speeds.

2.2.4. Water tank

The water volume stored in tanks (T1, T2 and T2) is given by the time integration of the difference between input and output flows. In fact, the tank water level $l(t)$ can be determined by:

$$\frac{dl(t)}{dt} = \frac{1}{S}\left(Q_{\text{in}}(t) - Q_{\text{out}}(t)\right). \tag{14}$$

where S is the surface area of a tank.

2.2.5. RO desalination unit

The inflow of the RO membrane module (FilmTec type BW 30-400) which passes the pump P2 from the tank T1 (feed flow Q_2) is converted from the freshwater flow (permeate Q_p) and the rejected water (concentrate Q_c) (Fig. 8). As the RO desalination process depends on many variables (raw water quality, permeate quality, feed temperature unit capacity, etc.), the authors use ROSA software (Reverse Osmosis System Analysis) to develop a model of the RO desalination unit. ROSA is used to design, sizing and simulation of the desalination plant equipped with FilmTec RO membranes [24]. In our case, compositions of brackish feed water in the Djerba Region (Southern Tunisia) were used (brackish water with a concentration of 6 g/L). The relation between the required electrical energy of the desalination pump and the amount of potable water produced is given with the help of ROSA software. In fact, the recovery rate characteristic vs. feed flow of the desalination process is presented in Fig. 9. With the help of ROSA software [24] for

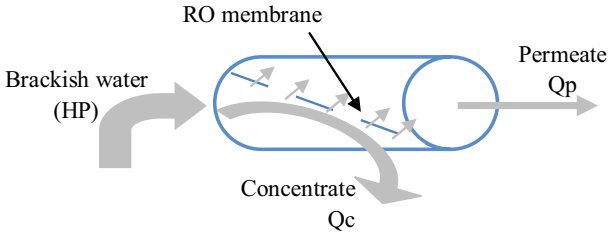

Fig. 8. RO membrane.

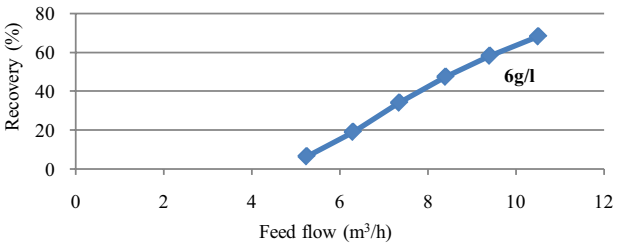

Fig. 9. Recovery rate vs. feed flow.

RO membrane (FilmTec) and using the "curve fitting tool" of MATLAB, the recovery–feed flow model can be given by:

$$\tau_R(\%) = 11.99 \times Q_2 - 55.42. \tag{15}$$

So, the model of the RO module can be expressed by:

$$Q_p = \tau_R \times Q_2. \tag{16}$$

where Q_2 and Q_p are respectively the feed flow from the pump P2 and the flow of the freshwater (permeate).

3. Integrated energy management

Energy management plays an important role to share the power flow during the system operation. The integrated power management is based on a set of conditions related to the produced hybrid power profile from renewable sources (P_{hyb}), the water level in tanks (l_i) and the electrical power range of the three motor-pumps ($P_{ei\_\min}$, $P_{ei\_\max}$). The system's operation is classified according to three main features: pumping, desalination and storage. Subsequently, these three features are divided into eight possible modes as shown in Fig. 10. Thereafter, in terms of input power (P_{hyb}) delivered by the hybrid source, the power range of different pumps and on the basis of eight modes selected, twelve operating regions ($Z_{i(i=0,\ldots,11)}$) were generated as shown in Fig. 11.

The choice of operation mode depends on the operating region (the power consumed by the motor-pumps) and the water level (l_1, l_2, l_3) in each tank. The water level is measured by different level sensors: low-level sensor (SL), medium level sensor (SM) and high-level sensor (SH). The medium-level sensor is defined by a hysteresis band: SM_H (higher level for the medium-level sensor) and SM_L (lower level for the medium-level sensor). A hysteresis band allows the prevention of ripple effects

(rapid and frequent start/stop) of pumps during the system operation. The operating zones are listed in Fig. 11 which Z_1 is defined by P_{e3_min} <= P_{hyb} < P_{e3_max}, Z_2 is defined by P_{e1_min} (or P_{e3_max}) <= P_{hyb} < P_{e2_min} (or P_{e1_min} + P_{e3_min}), etc.

Based on the different operating modes, the input power (P_{hyb}) is dispatched between pumps according to different power-sharing factors. For example, according to M3, if the pumps P1 and P3 are switched on, the power sharing factors are defined as:

$$\begin{cases}\alpha_{M3} = P_{e1\_min}/(P_{e1\_min} + P_{e3\_min}) \\ \beta_{M3} = P_{e3\_min}/(P_{e1\_min} + P_{e3\_min})\end{cases}. \quad (17)$$

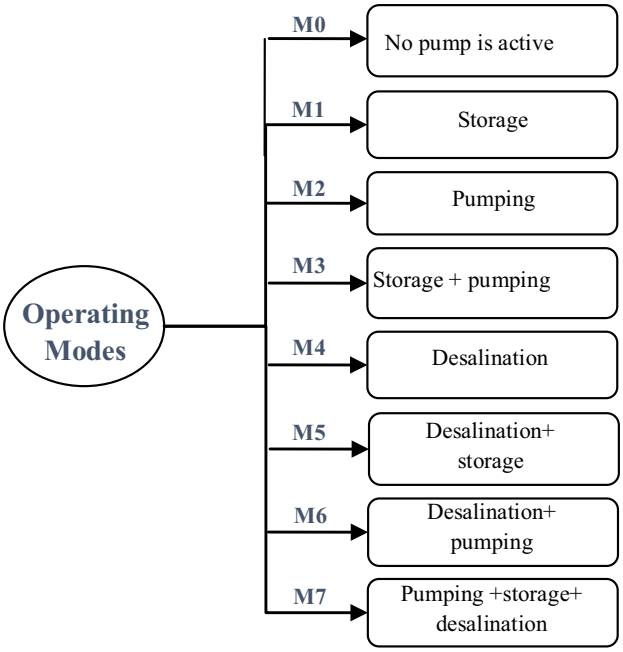

Fig. 10. Operating modes of the proposed energy management.

where P_{e1_min} is the minimum electrical power of motopump P1, P_{e3_min} is the minimum electrical power of motopump P3.

The input power (P_{hyb}) is similarly shared in the other modes. The input electrical power (P_{ei}) absorbed by the electric motor is derived from the mechanical power (P_{mi}), taking into account the motor and pump efficiency (η_{mi} and η_{pi} respectively).

4. Parametric sensitivity procedure

In this section, we present an approach to meet an Loss of Power Supply Probability (LPSP) = 0 of freshwater demand with the lowest primary energy requirement based on a sensitivity algorithm for sizing hydraulic process supplied by hybrid PV/wind system. In order to reduce environmental impact, primary energy requirement (PER) is presented as a criterion. A_{PV} (m²), A_{WT} (m²) and V_{Ri} (m³) will be the decision variables for sizing the studied system (V_{R1} is the BW tank (T1) capacity, V_{R2} is the permeate tank (T2) capacity and V_{R3} is the water tower (T3) capacity). In fact, the objective of the parametric sensitivity is to find the best configuration for the studied system (PV array area (A_{PV}), wind turbine (WT) swept area (A_{WT}) and tank storage capacity (V_{Ri})) with a minimum of embodied energy. Using the dynamic simulator, each combination of elements, once simulated, has been evaluated in terms of PER and LPSP thus making it possible to select the best one.

4.1. LCA indicators

4.1.1. Embodied energy of the PV-wind system

Primary energy requirement or embodied energy (EE) is the environmental indicator used to evaluate the environmental impacts of the proposed system [25,26]. The objective is to minimize the primary energy requirement cost ($PER_{PV/WT}$) of the hybrid source. The embodied energy

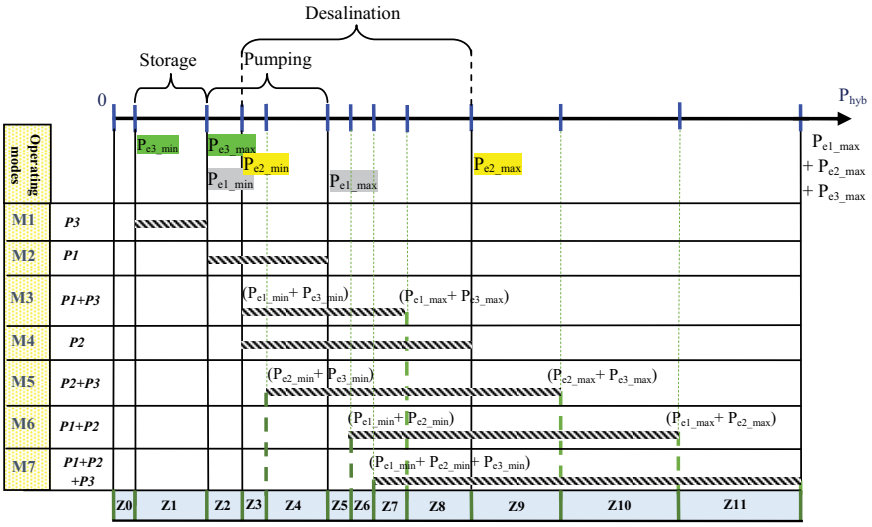

Fig. 11. Different operating modes are described by the proposed energy management.

criterion of the hybrid source (PV/wind) as a function of PV size (A_{PV}) and WT swept area (A_{WT}) is presented by Cherif et al. [27].

$$\mathrm{PER}_{PV/WT}\left(A_{PV}, A_{WT}\right) = \left(3863 \times A_{PV} - 47.26\right) + \left(2360 \times A_{WT} + 49.34\right) \quad (18)$$

4.1.2. Embodied energy of the hydraulic process

The objective is to minimize the primary energy requirement cost (PER_{HYD}) of the hydraulic process. The model of the hydraulic process is presented as a function of permeate flow rate (Q_p), the storage capacity of tanks (V_{R1}, V_{R2}, V_{R3}) and the size of the three motor-pumps. The embodied energy criterion of the hydraulic process is presented by Cherif et al. [27].

$$\begin{aligned}\mathrm{PER}_{HyP}\left(Q_p, V_{R1}, V_{R2}, V_{R3}, P_{e1}, P_{e2}, P_{e3}, P_{e\_SCV}\right) &= 5224.7 \times Q_p \\ +371.61 \times \left(V_{R1} + V_{R2}\right) &+ 1520 \times V_{R3} \\ +283.35 \times P_{e1} + 684.87 \times P_{e2} &+ 679.20 \times P_{e3} + 2200 \times P_{e\_SCV}\end{aligned} \quad (19)$$

4.1.3. Loss of power supply probability

The LPSP presents the system reliability and defines the probability that system demand will exceed the generating capacity during a given period. The reliability can be defined by Abbes et al. [28].

$$\mathrm{LPSP} = \frac{\sum_{t=1}^{T}\left|Q_{\mathrm{product}}(t) - Q_{\mathrm{demand}}(t)\right| \cdot \Delta t}{\sum_{t=1}^{T} Q_{\mathrm{demand}}(t) \cdot \Delta t} \quad (20)$$

where Q_{product} is the permeate flow product in the water tower, Q_{demand} is the permeate flow consumption (load demand to feed consumers). Note that LPSP is also considered if $l_3 \leq 0$: it is the hydraulic failure when the tank T3 is empty.

4.2. Dynamic simulator presentation

A dynamic simulator of a water pumping and desalination process supplied with a hybrid solar-wind production system as shown in Fig. 1 is developed. The dynamic simulator is based on a hybrid PV-wind power generator, reverse osmosis desalination unit, three motor-pumps (pump P1 for water pumping, pump P2 for water desalination process and pump P3 for water storage), three water tanks, integrated power management, energy calculator, the decision variables (PV array area, wind turbine swept area and capacity of storage tanks) and LCA indicators. Annual data of wind speed, solar irradiance and temperature from Southern Tunisia are used [29]. The meteorological data are programmed with a 10 min (sampling step) acquisition period for the full year of 2010 (52,560 points). In addition, real consumption data of freshwater were acquired in the month of November. The real profile of the freshwater demands was extrapolated for a full year considering seasonal variations using correction factors. 5,000 m³/y is the amount of annual water consumed.

4.3. Sensitivity assessment algorithm

Based on the decision variables (A_{PV}, A_{WT}, V_{R1}, V_{R2} and V_{R3}), the parametric sensitivity algorithm search to find the best compromise between two criteria: life cycle primary energy cost ($\mathrm{PER}_{PV/WT}$, PER_{HYD}) and LPSP. The developed algorithm is based on a dynamic simulator: each combination of elements, once simulated, has been evaluated in terms of embodied energy and LPSP thus making it possible to select the best one. The best configuration is predicted on the basis of the minimum of embodied energy with an LPSP equal to 0.

The ranges of decision variables are summarized in Table 1. Fig. 12 shows the LPSP as a function of PV array area (A_{PV} (m²)) and WT swept area (A_{WT} (m²)): it shows that the LPSP function is non-linear. The embodied energy of the PV/wind source vs. A_{PV} (m²) and A_{WT} (m²) is presented in Fig. 13. Fig. 14 shows a 3D representation of the embodied energy of the PV/wind source limited to LPSP = 0 as a function of A_{PV} (m²) and A_{WT} (m²). Fig. 15 shows a 4D representation of the embodied energy of the hydraulic process (PER_{HYD}) limited to LPSP = 0 as a function of V_{R1} (m³), V_{R2} (m³) and V_{R3} (m³). In order to give a clear curve, we limit the embodied energy (PER_{HYD}) of Fig. 15 to 1.95×10^5 MJ. The embodied energy limited to 1.95×10^5 MJ as a function of V_{R1} (m³), V_{R2} (m³) and V_{R3} (m³) with LPSP = 0 is presented in Fig. 16.

In fact, the chosen solution is given by the following configuration: photovoltaic modules' installed area A_{PV} = 96 m², WT swept area A_{WT} = 38 m², tanks' storage capacity V_{R1} = 20 m³, tanks storage capacity V_{R2} = 20 m³ and tanks storage capacity V_{R3} = 50 m³. This solution (for an entire life cycle) provides the lowest primary energy cost of the PV/wind source (462,400 MJ) and the lowest primary energy cost of the hydraulic process (192,710 MJ) for an LPSP equal to 0%.

This study allows us to determine the parameter's evolution range in order to limit them in the optimization process and consequently reduce the computation time.

5. GA optimization

In this section, a multi-objective optimization using genetic algorithm (GA) is investigated taking advantage of the parametric sensitivity study, in order to minimize

Table 1
Range of decision variables for parametric sensitivity

Parameter	Minimum values	Maximum values
A_{PV} (m²)	40	150
A_{WT} (m²)	10	40
V_{R1} (m³)	5	150
V_{R2} (m³)	5	150
V_{R3} (m³)	20	300

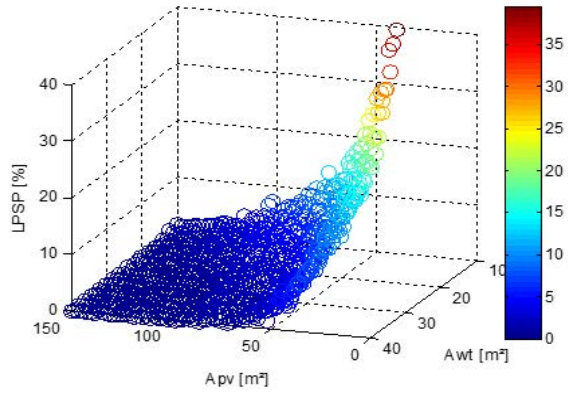

Fig. 12. LPSP of the hydraulic process vs. A_{PV} (m²) and A_{WT} (m²).

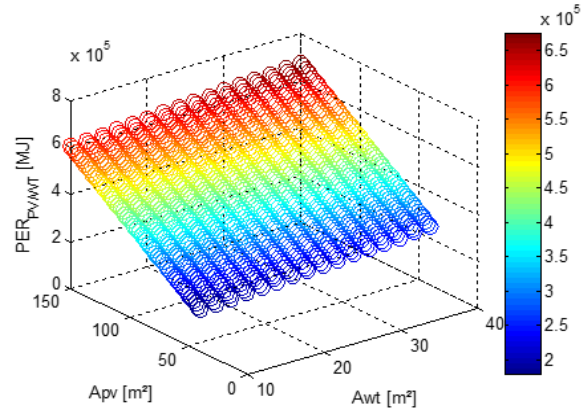

Fig. 13. Embodied energy of the PV/wind source vs. A_{PV} (m²) and A_{WT} (m²).

two objective functions: life cycle primary energy cost (MJ) and LPSP with five decision variables: PV array area (A_{PV} (m²)), wind turbine swept area (A_{WT} (m²)), the capacity of tank storage T1 (V_{R1} (m³)), the capacity of tank storage T2 (V_{R2} (m³)) and capacity of tank storage T3 (V_{R3} (m³)). NSGA-II (that is based on GA and Pareto dominance schemes) is an improved version of NSGA which overcomes many problems as the high computational complexity, limited elitism, and the need for parameter sharing. In our case, the multi-objective GA optimization is presented to satisfy the load demand LPSP and to reduce the environmental impacts (the investment energetic cost). The formulation of the optimization problem is given by El-Hana Bouchekara et al. [30].

$$\min x_i \begin{cases} F_1(x_i) = \text{PER} \\ F_2(x_i) = \text{LPSP} \end{cases} \quad (21)$$

The bounds of the decision variables set by the parametric sensibility study are presented in Table 2. As optimization results, the Pareto front of PER (MJ) and LPSP (%) is shown in Fig. 17. The simulation results show

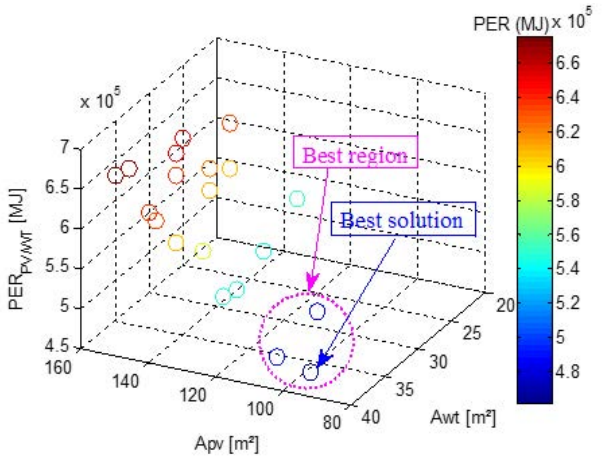

Fig. 14. Embodied energy of the PV/wind source with LPSP = 0.

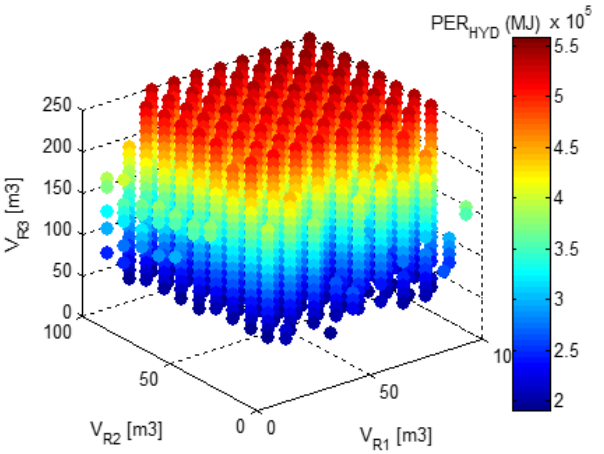

Fig. 15. Embodied energy of the hydraulic process with LPSP = 0 vs. V_{R1} (m³), V_{R2} (m³) and V_{R3} (m³).

that the parametric sensitivities-optimization method has proved very effective for the eco-design of the studied system in order to satisfy energy requirements from the hydraulic load with reduced environmental impacts. According to the evolution of the decision variables as a function of PER and LPSP, the new hybrid system configuration for an LPSP = 0% is composed of:

- PV modules' installed area A_{PV} = 89 m² (P_{PVmax} = 9.8 kW);
- Wind turbine swept area A_{WT} = 37 (P_{WTmax} = 8.85 kW) m²;
- Storage tanks capacity $V_{R1} = V_{R2}$ = 26 m³ and water tower capacity V_{R3} = 48 m³.

6. Results analysis

The hybrid system provides 100% of yearly freshwater needs. The amount of freshwater consumed for a year is about 5,000 m³/y. The average daily freshwater production is about 13.5 m³/d (brackish water has a salinity of 6 g/L). The water concentration range before (brackish water) and after (permeate water) the desalination process

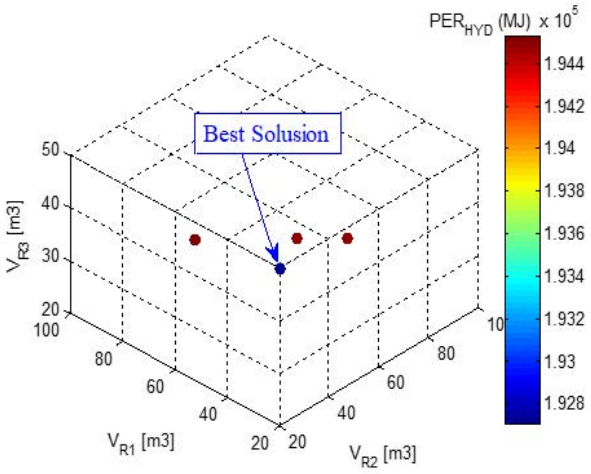

Fig. 16. Zoom on the embodied energy limited to 1.95×10^5 MJ vs. V_{R1} (m^3), V_{R2} (m^3) and V_{R3} (m^3) with LPSP = 0.

Table 2
Range of decision variables for optimization

Parameter	Minimum values	Maximum values
A_{PV} (m^2)	85	110
A_{WT} (m^2)	32	45
V_{R1} (m^3)	15	40
V_{R2} (m^3)	15	40
V_{R3} (m^3)	25	75

and the water concentration range is given by the World Health Organization (WHO) are presented in Table 3. A post-treatment phase must be used to regulate pH and total dissolved solids of the permeate water.

The optimal configuration can not only guarantee reliability (LPSP) but also reduce the investment energetic cost (PER). The results analysis has contributed to reducing the size of each element using a minimum of embodied energy with a better service for the user of water. The results showed that this sizing depends essentially on the volume of the water produced and not on the size of the water tanks. GA optimization-sensibility analysis nexus has shown good sizing efficiency using a minimum of primary energy cost with a better service for the user of water (LPSP equal to 0%). The results also show that the new modeling based on sensitivity analysis saves CPU time and accelerates the system simulation.

The embodied energy evaluation of the global system is summarized in Table 4. It is important to note that the total embodied energy for a life cycle period of 20 y of this hybrid system configuration is about 605,710 MJ (168,250 kWh). The total embodied energy is divided by 14% for wind turbine parts, 30% for hydraulic process and 56% for solar system components. The results showed that the embodied energy of 1 m^3 of freshwater is around 6 MJ. The authors give the last value with some reservation due that the embodied energy of 1 m^3 of freshwater is infrequently discussed in the literature.

As for recommendations, reduction of the total embodied energy of desalination processes may be achieved by the construction of plants near populated areas in order to eliminate the need for transportation of the product waters

Table 3
Water properties of brackish water permeate water and WHO requirement

Component	Brackish water (Southern Tunisia)	Permeate water	WHO requirements
pH	7.8	6.57	≥6.5 and ≤9.5
Total dissolved solids (mg/L)	5,401	187.58	<1,000
Sodium (mg/L)	1,430	61.34	200
Potassium (mg/L)	25.6	1.2	12
Calcium (mg/L)	320	4.17	<100
Magnesium (mg/L)	106	1.59	50
Ammonium (mg/L)	–	–	–
Strontium (mg/L)	–	–	–
Barium (mg/L)	–	–	–
Bicarbonate (mg/L)	167	–	–
Chloride (mg/L)	1,900	85.26	250
Sulfate (mg/L)	1,450	25.27	500
Fluoride (mg/L)	0	0	1.5
Nitrate (mg/L)	–	–	–
Silica (mg/L)	0	0	–
Boron (mg/L)	0	0	0.5
Iron and manganese (mg/L)	–	–	–

WHO: World Health Organization

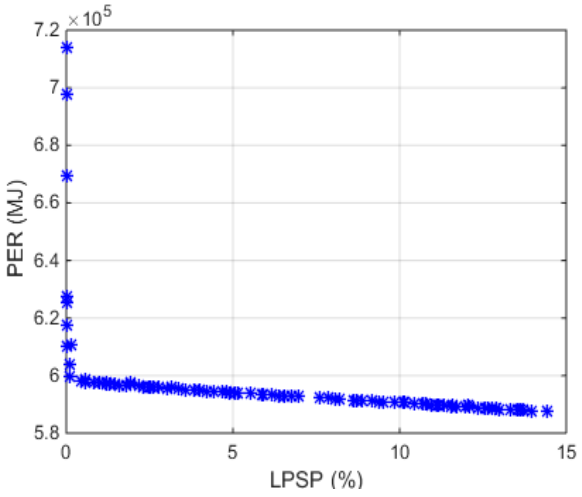

Fig. 17. Evolution of the two indicators PER and LPSP.

Table 4
LCA evaluation of the global system

System	Values
PER of the PV system (MJ)	333,800
PER of 1 m² of poly-Si PV panel (MJ/m²)	3,750
PER of the WT system (MJ)	89,200
PER of 1 m² of wind turbine (MJ/m²)	2,410
PER of the hydraulic system (MJ)	182,710
Total PER (MJ)	605,710
Total PER (kWh)	168,250
PER of 1 m³ of freshwater (MJ/m³)	6.1

for long distances and given priority to the development of desalination based on the use of renewable energy sources.

7. Conclusion

This paper presents a design methodology by GA optimization based on environmental life cycle analysis for sizing water pumping and desalination process coupled to renewable energy sources (PV/wind). The generated renewable energy is used to produce potable water by means of a reverse osmosis desalination unit. The dynamic simulator was developed using meteorological data (Southern Tunisia) for one year. To find the best configuration between PV array areas (A_{PV}), WT swept area (A_{WT}) and storage capacity of tanks (V_{Ri}), two criteria were used in optimization: primary energy requirement and LPSP. The approach consists of developing a parametric sensitivity study that has been integrated into optimization in order to determine the optimal operating zones which affect the optimization computation time. This approach provides good results and has shown good sizing efficiency for this type of system (water/energy) using a minimum of primary energy cost with a better service for the user of water (LPSP equal to 0%).

Acknowledgment

This work was supported by the Tunisian Ministry of High Education and Research under the ERANETMED-NEXUS "Energy and Water Systems Integration and Management" ID Number 14-044 for financial support.

References

[1] Z.X. Wang, X.N. Lin, N. Tong, Z.T. Li, S.T. Sun, C. Liu, Optimal planning of a 100% renewable energy island supply system based on the integration of a concentrating solar power plant and desalination units, Int. J. Electr. Power Energy Syst., 117 (2020) 105707, doi: 10.1016/j.ijepes.2019.105707.
[2] Y.P. Hua, M. Oliphant, E.J. Hu, Development of renewable energy in Australia and China: a comparison of policies and status, Renewable Energy, 85 (2016) 1044–1051.
[3] R. Hastik, S. Basso, C. Geitner, C. Haida, A. Poljanec, A. Portaccio, B. Vrščaj, C. Walzer, Renewable energies and ecosystem service impacts, Renewable Sustainable Energy Rev., 48 (2015) 608–623.
[4] K. Shivarama Krishna, K. Sathish Kumar, A review on hybrid renewable energy systems, Renewable Sustainable Energy Rev., 52 (2015) 907–916.
[5] S. Li, L. Gao, H.G. Jin, Life cycle energy use and GHG emission assessment of coal-based SNG and power cogeneration technology in China, Energy Convers. Manage., 112 (2016) 91–100.
[6] A. Khalilnejad, G.H. Riahy, A hybrid wind-PV system performance investigation for the purpose of maximum hydrogen production and storage using advanced alkaline electrolyzer, Energy Convers. Manage., 80 (2014) 398–406.
[7] M. Gökçek, Ö.B. Gökçek, Technical and economic evaluation of freshwater production from a wind-powered small-scale seawater reverse osmosis system (WP-SWRO), Desalination, 381 (2016) 47–57.
[8] N. Ghaffour, J. Bundschuh, H. Mahmoudi, M.F.A. Goosen, Renewable energy-driven desalination technologies: a comprehensive review on challenges and potential applications of integrated systems, Desalination, 356 (2015) 94–114.
[9] C. Gopal, M. Mohanraj, P. Chandramohan, P. Chandrasekar, Renewable energy source water pumping systems—a literature review, Renewable Sustainable Energy Rev., 25 (2013) 351–370.
[10] W.X. Peng, A. Maleki, M.A. Rosen, P. Azarikhah, Optimization of a hybrid system for solar-wind-based water desalination by reverse osmosis: comparison of approaches, Desalination, 442 (2018) 16–31.
[11] B. Zhou, B. Liu, D.S. Yang, J. Cao, T. Littler, Multi-objective optimal operation of coastal hydro-electrical energy system with seawater reverse osmosis desalination based on constrained NSGA-III, Energy Convers. Manage., 207 (2020) 112533, doi: 10.1016/j.enconman.2020.112533.
[12] H. Mehrjerdi, Modeling and optimization of an island water-energy nexus powered by a hybrid solar-wind renewable system, Energy, 197 (2020) 117217, doi: 10.1016/j.energy.2020.117217.
[13] A. Maleki, M.G. Khajeh, M.A. Rosen, Weather forecasting for optimization of a hybrid solar-wind–powered reverse osmosis water desalination system using a novel optimizer approach, Energy, 114 (2016) 1120–1134.
[14] G.Z. Zhang, B.J. Wu, A. Maleki, W.P. Zhang, Simulated annealing-chaotic search algorithm based optimization of reverse osmosis hybrid desalination system driven by wind and solar energies, Sol. Energy, 173 (2018) 964–975.
[15] R. Xavier, S. Bruno, N.D. Trung, B. Jamel, Optimal system management of a water pumping and desalination process supplied with intermittent renewable sources, IFAC Proc. Volumes, 45 (2012) 369–374.
[16] H. Cherif, J. Belhadj, Chapter 15 – Environmental Life Cycle Analysis of Water Desalination Processes, V.G. Gude, Ed., Sustainable Desalination Handbook: Plant Selection, Design and Implementation, Elsevier, Butterworth-Heinemann,

Woburn, MA, 2018, pp. 527–559. https://doi.org/10.1016/b978-0-12-809240-8.00015-0.
[17] M.T. Mito, X.H. Ma, H. Albuflasa, P.A. Davies, Reverse osmosis (RO) membrane desalination driven by wind and solar photovoltaic (PV) energy: state of the art and challenges for large-scale implementation, Renewable Sustainable Energy Rev., 112 (2019) 669–685.
[18] S. Miller, H. Shemer, R. Semiat, Energy and environmental issues in desalination, Desalination, 366 (2015) 2–8.
[19] A. Malekia, A. Askarzadeh, Comparative study of artificial intelligence techniques for sizing of a hydrogen-based stand-alone photovoltaic/wind hybrid system, Int. J. Hydrogen Energy, 39 (2014) 9973–9984. https://doi.org/10.1016/B978-0-12-374501-9.X0001-5.
[20] A.K. Soteris, Solar Energy Engineering: Processes and Systems, Elsevier, Burlington, 2009.
[21] A. Hysa, Modeling and simulation of the photovoltaic cells for different values of physical and environmental parameters, Emerging Sci. J., 3 (2019) 395–406.
[22] T.M. Layadi, G. Champenois, M. Mostefai, Modeling and design optimization of an autonomous multisource system under a permanent power-supply constraint, IEEE Trans. Sustainable Energy, 6 (2015) 872–880.
[23] Grundfos-WinCAPS Software, 2017. Available at: https://www.industrialgines.com/en/wincaps-7-43-grundfos/
[24] FilmTec releases ROSA Version 6.0, Membr. Technol., 2004 (2004) 3, doi: 10.1016/S0958-2118(04)00252-6.
[25] B. Guezuraga, R. Zauner, W. Pölz, Life cycle assessment of two different 2 MW class wind turbines, Renewable Energy, 37 (2012) 37–44.
[26] J.Q. Peng, L. Lu, H.X. Yang, Review on life cycle assessment of energy payback and greenhouse gas emission of solar photovoltaic systems, Renewable Sustainable Energy Rev., 19 (2013) 255–274.
[27] H. Cherif, G. Champenois, J. Belhadj, Environmental life cycle analysis of a water pumping and desalination process powered by intermittent renewable energy sources, Renewable Sustainable Energy Rev., 59 (2016) 1504–1513.
[28] D. Abbes, A. Martinez, G. Champenois, Life cycle cost, embodied energy and loss of power supply probability for the optimal design of hybrid power systems, Math. Comput. Simul., 98 (2014) 46–62.
[29] Metrological Data from a Tunisian Site. Available at: http://www.meteo.tn
[30] H.R. El-Hana Bouchekara, M.S. Javaid, Y.A. Shaaban, M.S. Shahriar, M.A.M. Ramli, Y. Latreche, Decomposition based multiobjective evolutionary algorithm for PV/wind/Diesel Hybrid Microgrid System design considering load uncertainty, Energy Rep., 7 (2021) 52–69.